Scientia Marina 88 (4)
December 2024, e092
ISSN-L: 0214-8358, eISSN: 1886-8134
https://doi.org/10.3989/scimar.05519.092

Relationships between the deep chlorophyll maximum and hydrographic characteristics across the Atlantic, Indian and Pacific oceans

Marta Estrada[1,9,10], Mikel Latasa[2], Ana M. Cabello[3], Patricia de la Fuente[4], Carles Guallar[5], Patricija Mozetič[6], Max Riera-Lorente[7], Montserrat Vidal[5], Dolors Blasco[8]

[1] Institut de Ciències del Mar, CSIC, Pg. Marítim de la Barceloneta, 37-49, 08003 Barcelona, Spain.
(ME) (Corresponding author) E-mail: marta@icm.csic.es. ORCID ID: https://orcid.org/0000-0001-5769-9498
[2] Centro Oceanográfico de Gijón/Xixón (IEO, CSIC), Avda. Príncipe de Asturias 70bis, 33212 Gijón/Xixón, Asturias, Spain.
(ML) E-mail: mikel.latasa@ieo.csic.es. ORCID ID: https://orcid.org/0000-0002-8202-0923
[3] Centro Oceanográfico de Málaga, Instituto Español de Oceanografía, IEO-CSIC, 29002 Málaga, Spain.
(AMC) E-mail: anamaria.cabello@ieo.csic.es. ORCID ID: https://orcid.org/0000-0002-7165-5632
[4] Laboratory of Human Evolution - IsoTOPIK Stable Isotope Laboratory, Department of History, Geography & Communication, Universidad de Burgos, Pl. Misael Bañuelos s/n, 09001, Burgos, Spain.
(PF) E-mail: pdelafuente@ubu.es. ORCID ID: https://orcid.org/0000-0002-6048-1534
[5] Departament de Biologia Evolutiva, Ecologia i Ciències Ambientals. Facultat de Biologia, Universitat de Barcelona (UB), Av. Diagonal, 643, 08028 Barcelona, Catalunya, Spain.
(CG) E-mail: cguallar@ub.edu, ORCID ID: https://orcid.org/0000-0001-7240-5873
(MV) E-mail: montsevidal@ub.edu. ORCID ID: https://orcid.org/0000-0002-7878-3290
[6] Nacionalni inštitut za biologijo / National Institute of Biology Morska biološka postaja Piran / Marine Biology Station Piran. Fornače 41, SI-6330 Piran, Slovenia.
(PM) E-mail: patricija.mozetic@nib.si. ORCID ID: https://orcid.org/0000-0002-4668-4511
[7] CFA La Verneda, Carrer d'Almacelles, 1, 08020 Barcelona, Spain.
(MR-L) E-mail: mriera50@xtec.cat. ORCID ID: https://orcid.org/0009-0006-0262-9349
[8] Retired. Previous address: Institut de Ciències del Mar, CSIC, Pg. Marítim de la Barceloneta, 37-49, 08003 Barcelona, Spain.
(DB) E-mail: blasco.@icm.csic.es
[9] Reial Acarèmia de Ciències i Arts de Barcelona
[10] Institut d'Estudis Catalans

Summary: The Malaspina-2010 circumnavigation expedition on board R/V *Hesperides* surveyed tropical and subtropical regions of the Atlantic, Indian and Pacific oceans between December 2010 and July 2011. This article examines the relationships between the distribution of chlorophyll *a* (Chl *a*), major inorganic nutrients and other hydrographic variables. A deep chlorophyll maximum (DCM) was found at most stations between 60 and 150 m depth; it occurred close to the level of 1% surface photosynthetically active radiation and was associated with the nitracline. There was a negative relationship between total Chl *a* at surface and the DCM depth, and between Chl *a* concentration at the DCM and DCM depth. In terms of Chl *a* concentration, picophytoplankton was the dominant size class at all sampled light intensities (surface, 20% of surface PAR and PAR at DCM), oceans and geoclimatic zones, except at some stations influenced by upwellings or divergences. Within the Chl *a* concentration ranges found in this study, the proportion of picophytoplankton increased with total Chl *a*, in contrast with some previous findings. Vertically integrated Chl *a* was positively correlated with surface Chl *a*, with similar slopes for the whole data set and for the different oceans and zones. In turn, surface Chl *a* and sea surface temperature showed a negative correlation for the Indian Ocean and the subtropical zone, a positive correlation for the Atlantic, and non-significant relationships for the remaining oceans and zones.

Keywords: Malaspina 2010; chlorophyll *a*; nitracline; deep chlorophyll maximum; phytoplankton size fractionation; Atlantic Ocean; Pacific Ocean; Indian Ocean.

Relaciones entre el máximo profundo de clorofila y las características hidrográficas en los océanos Atlántico, Índico y Pacífico

Resumen: Entre diciembre de 2010 y julio de 2011, la expedición de circunnavegación Malaspina-2010, a bordo del R/V Hespérides, estudió las regiones tropicales y subtropicales de los océanos Atlántico, Índico y Pacífico. Este trabajo examina las relaciones entre la distribución de la clorofila *a* (Chl *a*), los principales nutrientes inorgánicos y otras variables hidrográficas. En la mayoría de las estaciones, se encontró un máximo profundo de clorofila (MPC) entre 60 y 150 m de profundidad; se localizaba cerca del nivel del 1% de la radiación fotosintéticamente activa de superficie (PAR) y se asociaba con la nitraclina. Se encontró una relación negativa entre la Chl *a* total en superficie y la profundidad del MPC, y entre la concentración de Chl

a en el MPC y la profundidad del MPC. En términos de concentración de Chl *a*, el picofitoplancton fue la clase de tamaño dominante en todas las intensidades de luz muestreadas (de superficie, 20% de la PAR de superficie y PAR en el MPC), océanos y zonas geoclimáticas, excepto en algunas estaciones influidas por afloramientos o divergencias. Dentro de los rangos de concentración de Chl *a* encontrados en este estudio, la proporción de picofitoplancton aumentó con la Chl *a* total, en contraste con hallazgos de algunos trabajos anteriores. La Chl *a* integrada verticalmente se correlacionó positivamente con la Chl *a* superficial, con pendientes similares para todo el conjunto de datos y para los distintos océanos y zonas. A su vez, la Chl *a* y la temperatura superficiales presentaron una correlación negativa para el océano Índico y la zona subtropical, una correlación positiva para el Atlántico, y relaciones no significativas para el resto de océanos y zonas.

Palabras clave: Malaspina 2010; clorofila *a*; nitraclina; máximo profundo de clorofila; fraccionamiento por tamaño del fitoplancton; Océano Atlántico; Océano Pacífico; Océano Índico.

Citation/Como citar este artículo: Estrada M., Latasa M., Cabello A.M., de la Fuente P., Guallar C., Mozetič P., Riera-Lorente M., Vidal M., Blasco D. 2024. Relationships between the deep chlorophyll maximum and hydrographic characteristics across the Atlantic, Indian and Pacific oceans. Sci. Mar. 88(4): e092. https://doi.org/10.3989/scimar.05519.092

Editor: F. Peters.

Received: February 19, 2024. **Accepted:** September 25, 2024. **Published:** February 25, 2024.

INTRODUCTION

Oceanic phytoplankton is responsible for about half of the primary production on the planet and is a key component of biogeochemical cycles (Field et al. 1998). Remote sensing techniques have allowed an unprecedented view of surface distributions of biological properties in the oceans, such as chlorophyll *a* (Chl *a*) concentration. However, these tools are only capable of penetrating about 1 optical depth, while Chl *a* in oligotrophic marine regions [defined by Antoine et al. (1996) as those with Chl *a* concentrations <0.1 mg m^{-3}] shows vertical distributions in the water column with subsurface maxima out of the reach of the sensors. Oligotrophic regions featuring chlorophyll maxima at depths greater than 50 m comprise the subtropical gyres of the Atlantic, Pacific and Indian oceans, in addition to other areas such as the Mediterranean Sea, and occupy about 50% of the ocean surface (Mignot et al. 2014). The presence of deep chlorophyll maxima (DCM) in oligotrophic regions is related to water column stratification, which hinders the input of nutrients into the surface layers, so phytoplankton production is nutrient-limited in the upper euphotic zone and light-limited at depth (Cullen 2015). However, the intensity of the DCM and the precise depth at which it occurs are modulated by environmental and biological factors and therefore show both seasonal and geographical variations (Estrada et al. 1993, Cullen 2015). The DCM originates from a variable combination of enhanced cell biomass and increased Chl *a* per cell, due to both strengthened nutrient availability and photoacclimation to low light (Steele 1964, Latasa et al. 2005). The relative contribution of photoacclimation rises with increased oligotrophy, so in the more oligotrophic situations the DCM is due only or predominantly to increased Chl *a* per cell (Taylor et al. 2014, Cornec et al. 2021).

The relationship between integrated Chl *a* for the water column and stratification intensity is generally expected to be negative in temperate to tropical regions (Doney 2006). This idea has been challenged by Dave and Lozier (2013), who, based on in situ stratification measurements and remote sensing Chl *a* data, found no evidence of correlation between these variables in the subtropical ocean, although it existed for the tropical Pacific. Global warming is expected to increase ocean stratification, which in turn will modify Chl *a* concentration and distribution in the water column. Moreover, climate change may affect the functional group composition of the phytoplankton assemblages, including traits such as size class structure (Platt and Denman 1978, Finkel et al. 2010, Marañón 2015). Phytoplankton size may determine whether grazing is carried out by microzooplankton or by mesozooplankton, with implications for both the possibility of phytoplankton biomass accumulation and the relative importance of the microbial loop or of the classical food chain (Guidi et al. 2016). In addition, larger cells are expected to sink faster and contribute more to carbon export to the deep ocean (Barton et al. 2013). As the relative contribution of the various size classes of phytoplankton impacts food webs and the role of DCMs in biogeochemical cycles, it is imperative to gain insight on the mechanisms controlling these effects. A step towards this end consists in collecting measurements at large scales to characterize regional baselines and to test global relationships. In situ observations of chlorophyll profiles can also provide a crucial synergy with remote sensing observations, which have high spatial resolution but are limited to surface layers. The Malaspina-2010 circumnavigation expedition, on board the R/V *Hesperides*, which surveyed tropical and subtropical regions of the Atlantic, Indian and Pacific oceans through 15 biogeographic provinces, offered an excellent opportunity to obtain in vivo fluorescence profiles and to sample vertical Chl *a* distributions along a large geographical expanse. The cruise took place between December

2010 and July 2011, mostly during the spring-summer months of the visited regions (the main exception were the first ten stations, which were sampled in the northern hemisphere winter), thus minimizing seasonal variability, and included 147 oceanographic stations, many of them in poorly sampled areas. The same methods were used throughout, ensuring comparability of the results (Moreno-Ostos et al. 2012).

A previous article (Estrada et al. 2016) described some general features of the Chl *a* distribution during the Malaspina expedition, in connection with the composition of the nano- and microphytoplankton community as determined by optical microscopy. The present article examines in detail the vertical distribution of Chl *a* and the relationships between hydrographic variables and the characteristics of the DCM during Malaspina. In particular, we aim to 1) assess the geographical variability of the vertical Chl *a* profiles and their relationships with vertical markers such as irradiance intensity and the nutricline and mixed layer depths, 2) evaluate the contribution of micro-, nano- and picophytoplankton to total Chl *a*, in relationship with environmental properties, and use these observations to test existing algorithms such as that of Hirata et al. (2011), and 3) explore the relationships of surface and water column-integrated Chl *a* with sea surface temperature and stratification.

MATERIAL AND METHODS

Sampling strategy and physical measurements

The Malaspina-2010 cruise crossed tropical, subtropical and temperate oceans around the globe between 35°N and 40°S in seven consecutive legs (Fig. 1). The cruise started and ended in Cartagena, Spain, and crossed the Atlantic, Indian and Pacific oceans (Tables S1 and S2). To summarize information for some analyses performed in this work, a loose latitudinal classification into coastal, and equatorial, subtropical and tropical open ocean geoclimatic zones was adopted (Table S1).

At each station, two or more vertical profiles of conductivity-temperature-depth (CTD) were obtained with a CTD SeaBird 9/11-plus equipped with additional sensors of dissolved oxygen concentration, turbidity, fluorescence, light transmission, underwater photosynthetically active radiation (PAR), surface irradiance and bottom proximity (measured using an altimeter). During the second CTD cast, which started around 10:00 local time, water samples for determination of total Chl *a* and nutrient concentrations were collected from the surface (3 m depth) by means of a 30-litre Niskin bottle and from 9 additional depths using 12-litre Niskin bottles mounted on a "rosette". In general, these 9 depths included 10 m, the depths of 50% and 20% of surface PAR, an "intermediate depth 1", the depth of 7% surface PAR, an "intermediate depth 2", the DCM depth (as determined from the CTD profile), the DCM depth + 20 m and the DCM depth + 50 m.

The mixed layer depth (MLD) was calculated as the first depth (z) for which $\sigma_\theta(z)-\sigma_\theta(10)\geq 0.125$ kg m^{-3}, where $\sigma_\theta(z)$ and $\sigma_\theta(10)$ are, respectively, the potential density anomalies at depths z and 10 m (Levitus 1982). The stratification profile of the water column was characterized by means of the Brunt-Väisälä (B-V) frequency (N^2), calculated at 2 m intervals. The strength of stratification in the upper 200 m was estimated as

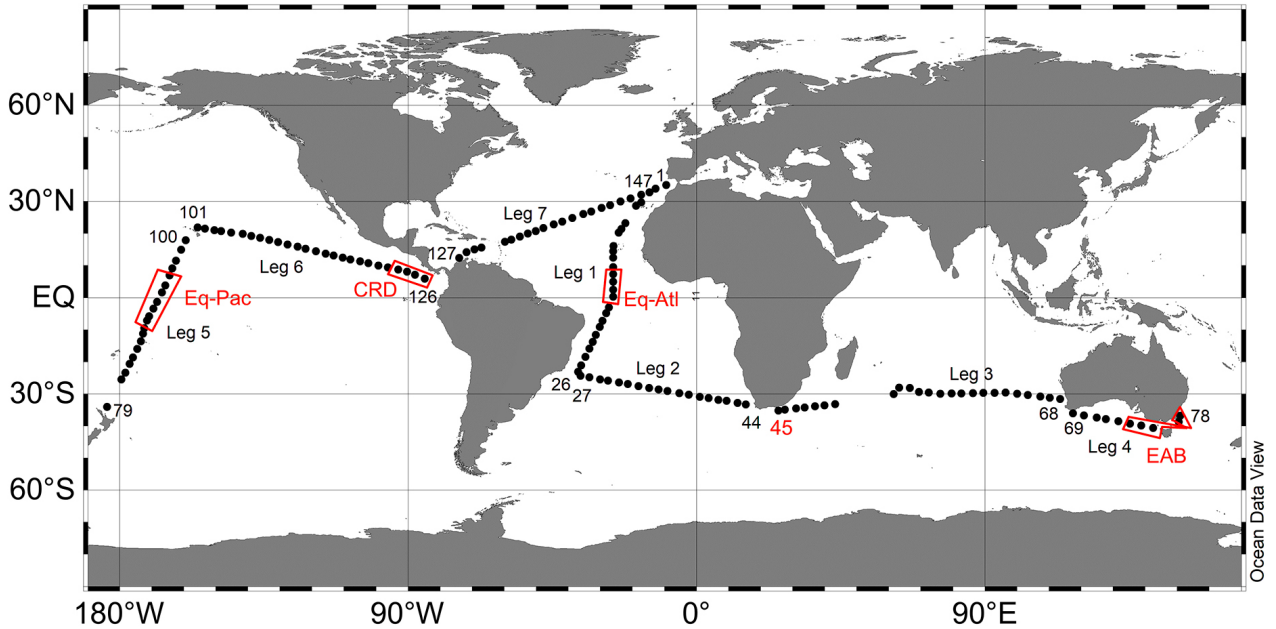

Fig. 1. – Cruise track of the Malaspina-2010 expedition. The numbers along the tracks designate the first and last stations of each leg. Red boxes and labels indicate regions with upwellings or divergences. Eq-Pac, Pacific equatorial upwelling; Eq-Atl, Atlantic equatorial upwelling; CRD, Costa Rica Dome; 45, Station 45 (Agulhas Current region); EAB, Eastern Great Australian Bight.

$\sigma_\theta(200)$-$\sigma_\theta(6)$ (hereafter σ200-σ6), the difference between the potential density anomalies (with reference pressure of 0 dbar) at 200 and at 6 m depth (Behrenfeld et al, 2006). The euphotic zone depth was considered to be the depth of 1% of the surface irradiance, calculated from the PAR CTD records. The Ocean Data View software (Schlitzer 2023) was used to present the distribution of hydrographical variables and to calculate B-V frequencies and potential density anomalies.

Chlorophyll *a* and nutrient analyses

Analysis of total Chl *a* (Chl *a*_tot) was performed for samples taken between the surface (3 m depth) and 50 m below the DCM depth. From 250 to 500 mL of seawater were filtered through 25 mm GF/F filters, which were frozen for about 6 hours at 20°C, introduced in acetone 90% and left for 24 hours at 4°C in the dark. The Chl *a* concentration in the acetonic extracts was determined fluorometrically with a Turner Designs fluorometer calibrated with pure Chl *a* (Sigma-Aldrich). Size-fractionated analyses of Chl *a* were carried out for samples from the surface, the 20% surface PAR and a deeper depth that in general coincided with the DCM depth [the main exceptions were stations 45 (Agulhas Current region), 16 (Atlantic equatorial upwelling) and 90-96 (Pacific equatorial upwelling), which did not show a DCM]. Stations at which the deeper fractionation depth differed by more than 10 m from the DCM depth were excluded from the DCM calculations in Table 2. The measurements were performed by sequential filtration through 47 mm Poretics polycarbonate membrane filters of 20, 2 and 0.2 µm pore sizes, which were subsequently treated as the GF/F ones (Estrada 2012, Estrada et al. 2016). The fractional contribution of microphytoplankton (f_micro, >20 µm), nanophytoplankton (f_nano, >2 and <20 µm) and picophytoplankton (f_pico, >0.2 and <2 µm) was calculated with respect to the sum of Chl *a* in the three size fractions (Chl *a*_pol), which tended to be slightly lower than the total Chl *a* determined by filtration onto GF/F filters (Chl *a*_pol=0.91*Chl *a*_tot - 0.21, r^2=0.87, p<0.0001). For comparison, the relative contribution of the three phytoplankton size fractions (f_micro, f_nano and f_pico) was also estimated by means of the Chl *a*–based approach of Hirata et al. (2008, 2011):

f_micro $[0.9117+\exp(-2.733x + 0.4003)]^{-1}$
f_nano 1-f_micro-f_pico
f_pico $-[0.1529+\exp(1.0306x-1.5576)]^{-1}-1.8597x + 2.9954$,

where x=log10(Chl *a*_tot)

The possibility of fitting the three-component model of Brewin et al. (2010, 2014), which derives the fractions of picophytoplankton (<2 µm) and combined pico- and nanophytoplankton (<20 µm) chlorophyll with total chlorophyll concentration, was examined, but our data could not be adjusted to the model equations because these include a parameter representing an asymptotic maximum chlorophyll concentration for the <2 µm and <20 µm size classes that was not reached in our data set.

Nutrient (silicate, nitrate, nitrite and phosphate) concentrations were determined by means of a Skalar autoanalyser, using standard spectrophotometric procedures (Grasshoff et al. 1999, Blasco et al. 2012); in leg 1, nitrite was not determined, and phosphate was measured using a manual method (Vidal et al. 2012). The nutricline depth was represented by that of the nitracline, which was defined as the depth at which nitrate (nitrate + nitrite in leg 1) concentrations first reached 1 mmol m^{-3}; in most cases, it was determined by linear interpolation based on the closest samples encompassing this threshold. Some stations (mostly from the Pacific equatorial upwelling) with nitrate concentrations at surface exceeding 1 mmol m^{-3} did not have a nitracline depth. In a few others, the calculated nitracline depth was slightly shallower than the MLD but was considered to be equal to the MLD. This was done because the limited number of vertical nutrient samples precluded a fine depth resolution and it was assumed that, in stratified conditions, a nitracline would not occur within the mixed layer. Different nutricline depths could be obtained if calculated from phosphate, but we chose nitrate because nitrogen is considered to be the main limiting nutrient in stratified subtropical gyres (Browning and Moore 2023).

Calculation of high-resolution chlorophyll *a* profiles

Chl *a* profiles matching the CTD records (available at 1 or 2 m intervals) were obtained as described in Estrada et al. (2014). First, CTD in situ fluorescence readings were converted to Chl *a* concentrations (hereafter Chl *a*_CTD) based on calibration equations obtained for each leg from the regression of Chl *a*_tot values measured in the ship laboratory vs. in situ fluorescence readings corresponding to the same depth. Chl *a*_tot concentration between 0 m and 10 m depth was assumed to be equal to Chl *a*_tot concentration at 3 m. Second, a linear interpolation (Chl *a*_tot-int) of Chl *a*_tot based on the closest available Chl *a*_tot above and below the interpolation depths was assigned to each depth of the high-resolution (1–2 m intervals) vertical CTD profiles between 10 m and the DCM + 50 depths. Third, a similar interpolation procedure was carried for Chl *a*_CTD to calculate Chl *a*_CTD-int based on the Chl *a*_CTD values of the same depths adopted to interpolate Chl *a*_tot. Fourth, we multiplied the interpolated Chl *a*_tot-int at each depth by a correction factor consisting of the ratio between the Chl *a*_CTD derived from the actual in vivo fluorescence reading and the linearly interpolated Chl *a*_CTD-int for this depth. This correction factor was introduced to compensate for non-linearity of the Chl *a* profiles and was based on the assumption that, at subsurface depths, in situ fluorescence would be proportional to Chl *a* concentration. Integrated Chl *a* between 0 and 200 m depth (Chl *a*_int) was then computed using the trapezoidal rule (for this calculation, Chl *a* between the DCM + 50 and 200 m was supposed to be equal to the corresponding Chl *a*_CTD).

Statistical analyses and data availability

Linear regressions and correlation coefficients were calculated using the Systat 13 software. A *t* test was used to estimate the significance of differences among regression slopes (Paternoster et al. 1998). The distribution of size class fractions among light levels and oceans or geoclimatic zones was evaluated with a two-way ANOVA followed by post-hoc Tuckey tests, using the Systat software. Chl *a* concentration values were log-transformed to approximate the distributions to normality. Since our interest was to quantify the pattern of covariation rather than to carry out an estimation of the dependent variables, the analysis of the bivariate linear relationships between the Chl *a* size fractions and Chl *a*_pol was carried out with the reduced major axis regression model (RMA), using the PAST4 software (https://www.nhm.uio.no/english/research/resources/past/). In this way, we also tried to minimize the influence of the different degrees of dispersion of the data around the regression lines. Chl *a* (http://hdl.handle.net/10261/345389) and nutrient (https://doi.org/10.20350/digitalCSIC/16127) data are available at Digital CSIC (www.digital.csic.es).

RESULTS

Distribution and characteristics of the Deep Chlorophyll Maximum

Chl *a*_tot concentrations encountered during the Malaspina expedition (Fig. 2) ranged from 0.03 to 0.69 mg m^{-3} at surface (3 m depth), from 0.05 to 1.08 mg m^{-3} at the 20% light level and from 0.11 to 1.92 mg m^{-3} at the DCM. Among oceans, average Chl *a*_tot values ranged from 0.12 mg m^{-3} in the Atlantic to 0.21 mg m^{-3} in the Pacific at surface and from 0.42 mg m^{-3} in the Indian to 0.5 mg m^{-3} in the Pacific at the DCM (Table 1). By geoclimatic zones, average Chl *a*_tot went from 0.10 mg m^{-3} in the subtropical zone to 0.30 mg m^{-3} in the equatorial at surface and from 0.38 mg m^{-3} in the subtropical zone to 0.68 mg m^{-3} in the coastal zone for the DCM (Table 1). In general, there was a marked temperature stratification, with MLDs ranging between 40 and 100 m (Fig. 2A). The seasonal changes between the North Atlantic crossings of legs 1 and 7 were reflected in higher sea surface temperatures and shallower MLDs in the later leg. The thinnest MLDs and the highest surface Chl *a* (Chl *a*_srf) concentrations were found (Figs 1 and 2) in regions such as the equatorial upwelling zone of the Atlantic, the Costa Rica or Mesoamerican Dome and the eastern coast of South Africa (Agulhas Current, station 45). Another zone with relatively high Chl *a* concentrations was the Eastern Great Australian Bight, which showed a cool, deep (MLD of 60–80 m) mixed layer on top of a dome of relatively cold water (Fig. 2). This situation was accompanied by a high contribution of *Prochlorococcus* and a homogeneous vertical distribution of phytoplankton, suggesting an early autumn mixing event (Latasa et al. 2023).

Most stations showed a DCM between 60 and 150 m depth, close to the level of 1% surface PAR (Figs 2 and 3A). In general, the DCM was deeper than the MLD (Fig. 3B) and was either absent or above 40–60 m in regions influenced by upwelling or divergences, such as the equatorial upwellings, the Costa Rica

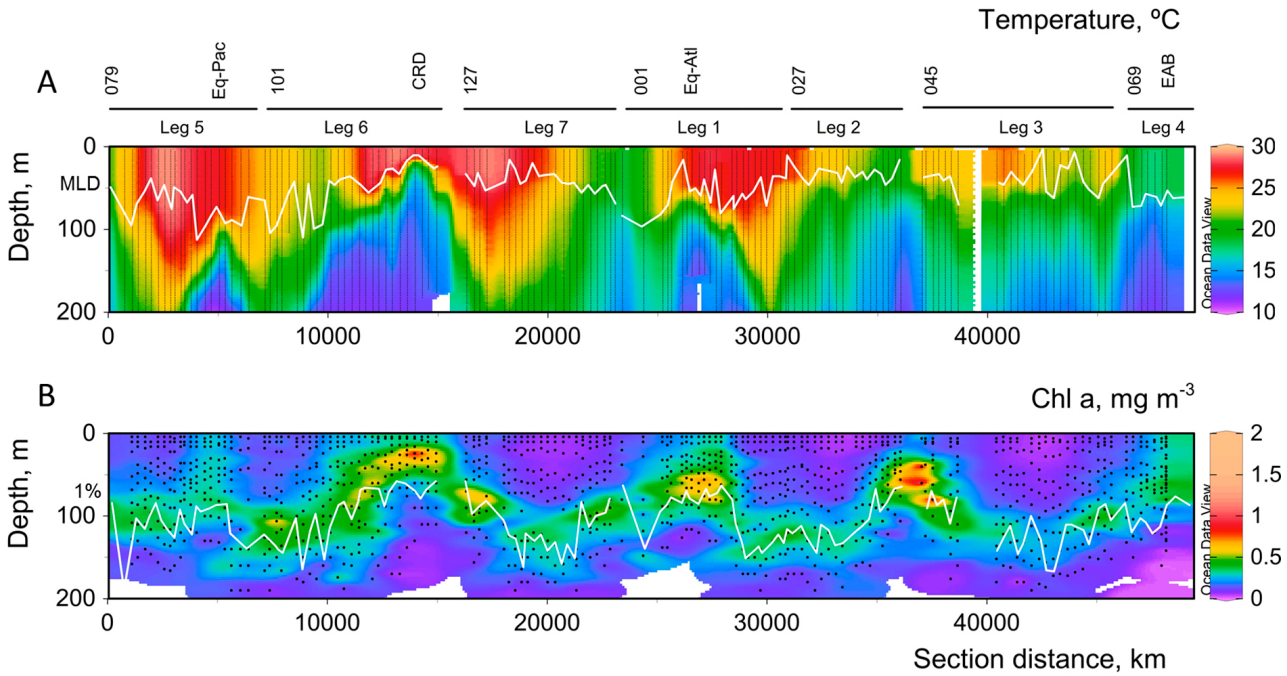

Fig. 2. – Temperature and Chl *a* distributions during the Malaspina-2010 expedition. (A) Temperature, °C. (B) Chl *a*, mg m^{-3}. The white lines indicate the mixed layer depth (labelled "MLD") in (A) and the 1% light level (labelled "1%") in (B). The initial and final stations of each leg and the different regions indicated in Figure 1 are shown at the top of the (A) panel.

Table 1. – Average (mean±sd) values of Chl *a* concentration at surface (Chl *a*_srf) and at the DCM (Chl *a*_DCM), integrated Chl *a* from surface down to 200 m (Chl *a*_int), average DCM depth and difference between the potential density anomalies at 200 m and 6 m depth (σ200-σ6) for the oceans and zones and for the whole data set; N is the number of observations.

Oceans	Chl *a*_srf, mg m^{-3}	Chl *a*_DCM, mg m^{-3}	Chl *a*_int, mg m^{-2}	DCM depth, m	σ200-σ6 kg m^{-3}	N
Atlantic	0.12±0.11	0.50±0.20	37.08±9.46	108.4±31.4	1.77±0.91	55-61
Indian	0.15±0.14	0.42±0.18	34.26±14.38	102.1±26.1	1.83±0.58	32-34
Pacific	0.21±0.12	0.53±0.25	45.92±11.81	86.4±38.5	3.03±1.27	38-45
All	0.16±0.13	0.49±0.21	39.31±12.38	100.4±33.6	2.20±1.33	129-141
Zones						
Equatorial	0.30±0.13	0.66±0.30	49.35±12.16	53.74±24.77	4.08±0.92	19-27*
Tropical	0.15±0.09	0.47±0.14	42.67±11.95	110.10±31.0	2.20±0.82	29-32
Subtropical	0.10±0.08	0.38±0.10	32.34±5.37	114.4±24.2	1.65±0.71	64-66
Coastal	0.19±0.15	0.68±0.21	43.71±17.41	79.6±17.2	2.29±0.91	15-16

*There was no DCM at equatorial upwelling stations 16 (Atlantic) and 90–96 (Pacific)

Dome and the Eastern Great Australian Bight. For simplicity, these areas will be subsequently designated as upwelling-divergence (U-D) regions, as in Estrada et al. (2016). The DCM appeared well below the depth of maximum B-V frequency (data not shown) in the open Indian Ocean and tropical and subtropical Pacific, and was found near the maximum B-V frequency depth in the U-D regions.

The linear regression equations of DCM depth on nitracline depth were positive and significant ($p<0.001$) and had similar slopes for all three oceans (Table S3). Above 100 m depth, the nitracline and the DCM depth were approximately aligned in a 1:1 relationship, but below 100 m the DCM tended to be shallower than the nitracline (Fig. 4A). When the data were categorized according to geoclimatic zones, the slopes of the relationship decreased from the equatorial to the tropical and the subtropical zones, with intermediate values for the coastal samples (Table S3); however, only the difference between the equatorial and the subtropical zones was significant at the $p<0.05$ level. The nitrite maximum depth was in general deeper or coincident with the DCM depth, and both parameters were significantly correlated with fairly similar regression slopes for all three oceans (Fig. 4B), although the low vertical resolution of the nutrient sampling originated a substantial dispersion of the points. There was a negative relationship between total Chl *a* at surface (Chl_*a*_srf) and DCM depth, with slopes that were more negative for the Pacific than for the Atlantic and Indian oceans, according to the *t* test (Fig. 5A, Table S4). Chl *a*_tot concentration at the DCM (Chl *a*_DCM) was negatively correlated with the DCM depth (Fig. 5B, Table S4), with similar slopes for all oceans.

Relationships between total and size-fractionated chlorophyll *a*

The proportion of picophytoplankton Chl *a* (f_pico) (Table 2) was significantly higher at the DCM, with mean values (expressed in percentages) around 70%, than at surface and the 20% light levels, where it ranged between 49% and 60% (two-way ANOVA, $p<0.0001$). Among oceans, the Atlantic showed lower f_pico values than the Indian and Pacific, in particular at surface and 20% PAR (two-way ANOVA, $p<0.001$). The mean proportion of nanophytoplankton (f_nano, Table 2) ranged from 24% to 38%, was lower at the DCM than at surface and the 20% light levels (two-way ANOVA, $p<0.0001$) and showed no significant differences between oceans. The relative contribution of the microplankton (f_micro, Table 2) showed ranges (expressed in percentages) from 6% to 14% at the upper two light levels and from 4% to 6% at the DCM and was significantly different between light levels (lower values at the DCM) and oceans (two-way ANOVA, $p<0.0001$); the lowest overall values corresponded to the Indian Ocean.

The slopes of the RMA linear regressions of the log-transformed Chl *a* concentration of pico-, nano- and microphytoplankton versus the log-transformed Chl *a*_pol (the sum of the three fractions measured on polycarbonate filters) for the separate and combined light levels ranged between 0.98 and 1.49 (Table S5). Nanophytoplankton showed the lowest slope for surface, the 20% light level and the pooled data, while the slopes of micro- and picophytoplankton were not significantly different (Fig. 6, Table S5A). The same pattern was found when Chl *a*_tot (from GF/F filters) was used instead of Chl *a*_pol (data not shown). The correlation coefficients between the proportions of the three size classes (f_micro, f_nano and f_micro) and Chl *a*_pol (Table S5B) were in general significant but r^2 did not exceed 0.23. The RMA regression of f_pico on log(Chl *a*_pol) had a positive slope for all light levels, while the RMA regressions of f_nano on log(Chl *a*_pol) were all negative and those of f_micro were either non-significant (for the surface and the 20% light level) or negative (for the DCM and the whole data set) (Fig. S1, Table S5B). Neither f_pico nor f_nano were signifi-

Table 2. – Mean, sd and number of observations (N) of the fractional (per unit) contributions of micro- (f_micro), nano- (f_nano) and picophytoplankton (f_pico) to total Chl *a* for the oceans and zones and for the whole data set ("All").

		Surface			20% PAR			DCM		
	Oceans	Mean	sd	N	Mean	sd	N	Mean	sd	N
f_pico	Atlantic	0.54	0.16	59	0.49	0.13	56	0.69	0.13	44
	Indian	0.60	0.10	31	0.58	0.14	29	0.70	0.10	28
	Pacific	0.60	0.14	45	0.60	0.13	43	0.70	0.11	27
	All	0.57	0.14	135	0.55	0.14	128	0.69	0.12	99
f_nano	Atlantic	0.33	0.14	59	0.38	0.13	56	0.25	0.12	44
	Indian	0.34	0.09	31	0.35	0.14	29	0.25	0.09	28
	Pacific	0.31	0.12	45	0.31	0.11	43	0.24	0.10	27
	All	0.33	0.12	135	0.35	0.13	128	0.25	0.11	99
f_micro	Atlantic	0.14	0.09	59	0.13	0.11	56	0.06	0.03	44
	Indian	0.06	0.03	31	0.07	0.08	29	0.04	0.02	28
	Pacific	0.08	0.08	45	0.09	0.08	43	0.06	0.03	27
	All	0.10	0.09	135	0.1	0.1	128	0.05	0.03	99
	Zones									
f_pico	Equatorial	0.59	0.18	27	0.58	0.13	26	0.64	0.13	15
	Tropical	0.62	0.13	30	0.55	0.18	28	0.73	0.10	21
	Subtropical	0.53	0.12	62	0.60	0.13	60	0.71	0.11	49
	Coastal	0.59	0.12	16	0.58	0.13	14	0.66	0.14	14
f_nano	Equatorial	0.30	0.16	27	0.33	0.13	26	0.30	0.12	15
	Tropical	0.28	0.11	30	0.35	0.15	28	0.21	0.08	21
	Subtropical	0.37	0.11	62	0.31	0.11	60	0.24	0.10	49
	Coastal	0.31	0.10	16	0.29	0.15	14	0.30	0.13	14
f_micro	Equatorial	0.11	0.09	27	0.10	0.07	26	0.06	0.02	15
	Tropical	0.10	0.08	30	0.10	0.11	28	0.06	0.03	21
	Subtropical	0.10	0.10	62	0.09	0.08	60	0.05	0.03	49
	Coastal	0.09	0.07	16	0.13	0.14	14	0.04	0.02	14

cantly correlated with temperature (whether for separate light levels or the whole data set, data not shown). Only f_micro showed a significant but low correlation with temperature for the surface and the 20% light levels (Spearman correlation coefficients of 0.45 and 0.48, respectively, for n=127 -136).

For all light levels, the correlation coefficients between the measured micro- and picophytoplankton proportions (f_micro and f_pico, respectively) and those derived from the Hirata (2011) equations (Fig. S2) were significant, although with low r^2 (0.03 and 0.22, respectively, $p<0.001$). When light levels were considered separately (data not shown), only the correlation between the picophytoplankton proportions remained significant, but also with low r^2 ($r^2=0.15$, $p<0.001$, $r^2=0.14$, $p<0.001$ and $r^2=0.06$, $p<0.005$, for surface, 20% and the DCM, respectively).

Relationships of integrated chlorophyll *a* (Chl *a*_int) with surface chlorophyll *a* (Chl *a*_srf), surface temperature and stratification

Surface temperature (SST) and stratification (σ200-σ6) were positively correlated for all oceans and regions (Table 3). Integrated Chl *a* (Chl *a*_int) values between surface and 200 m depth (Fig. S3) ranged from 19 mg m^{-2} at station 141, in the subtropical North Atlantic, to 101 mg m^{-2} at station 45, near the East African coast (Agulhas Current region). The correlations between the logarithms of Chl *a*_int and Chl *a*_srf were

Table 3. – Linear correlation coefficients between sea surface temperature (SST), the stratification index σ200-σ6 and the logarithms of surface [log(Chl *a*_srf)] and integrated Chl *a* concentration ([log(Chl *a*_int] for the oceans and zones and for the whole data set ("All"). N = number of observations. * $p<0.05$.

	SST with		log(Chl *a*_srf) with						log(Chl *a*_int) with			
Oceans												
	σ200-σ6	N	SST (ºC)	N	σ200-σ6	N	log(Chl *a*_srf)	N	SST (ºC)	N	σ200-σ6	N
Atlantic	0.80*	55	0.32*	61	0.40*	54	0.69*	56	0.17	56	0.38*	54
Indian	0.90*	34	-0.53*	34	-0.38*	34	0.62*	32	0.11	32	0.14	32
Pacific	0.72*	43	0.23	46	0.63*	42	0.48*	42	-0.13	42	0.24	42
All	0.73*	132	0.15	141	0.47*	130	0.66*	130	0.25*	130	0.43*	128
Zones												
	σ200-σ6	N	SST (ºC)	N	σ200-σ6	N	log(Chl *a*_srf)	N	SST (ºC)	N	σ200-σ6	N
Equatorial	0.55*	19	-0.04	27	0.74*	19	0.54*	20	-0.15	20	0.3	19
Tropical	0.44*	29	-0.24	32	0.32	29	0.52*	30	-0.48*	30	0.2	29
Subtropical	0.73*	68	-0.32*	66	-0.11	66	0.46*	64	0.27*	64	0.17	64
Coastal	0.95*	16	-0.09	16	-0.0009	16	0.58	16	-0.05	16	-0.01	16

significant ($p<0.05$) for the whole data set and for the different oceans and geographical zones except for the coast (Table 3). Linear regression slopes of Chl *a*_int on Chl *a*_srf were not significantly different among oceans and zones (Fig. 7A, Table S4). Log(Chl *a*_srf) showed a significant positive correlation with SST for the Atlantic and negative correlations for the Indian Ocean and the subtropical region; log(Chl *a*_srf) and σ200-σ6 were also negatively correlated for the Indian Ocean, but showed significant positive correlations for the other oceans and the equatorial zone. Log(Chl *a*_int) was negatively correlated with SST for the tropical region; the remaining relationships between log(Chl *a*_int) with SST and σ200-σ6 for other oceans and zones were either positive or non-significant (Fig. 7B, Table 3).

DISCUSSION

Distribution and characteristics of the deep chlorophyll maximum

The Malaspina cruise visited tropical and subtropical regions of the northern and southern hemispheres in general during the corresponding spring-summer period, so most stations showed stratified water columns with wide MLDs and nitraclines below 50 m. These conditions are typically associated with low Chl *a* concentrations at surface (from 0.03 to 0.69 mg m^{-3}) and vertical profile features such as deep chlorophyll and nitrite maxima. Locations with shallow MLDs and nitraclines and with relatively high Chl *a*_srf concentrations, which deviated from this pattern, were those associated with upwellings or divergences in the U-D regions (Figs 2, S4) and included stations 90–96 (Pacific equatorial upwelling), 13–16 (Atlantic equatorial upwelling), 45 (Agulhas Current), 123–126 (Costa Rica or Mesoamerican Dome) and 74–78 (Eastern Great Australian Bight). The presence of these U-D zones resulted in higher average Chl *a*_srf and shallower average DCMs (Table 1) in the Pacific Ocean and the equatorial zone than in the other areas, as found in previous works (Weingartner and Weisberg 1991, Wyrtki 1981, Fiedler and Talley 2006, van Ruth et al. 2018). However, even in U-D areas, only five samples from the 20% and DCM depths (from stations 13, 44–45 and 122) had Chl *a* concentrations exceeding 1 mg m^{-3}. As found in previous surveys (Zhang et al. 2012), both Chl *a*_srf and Chl *a*_int were higher at the eastern (stations 79–90) than at the central Pacific ones (stations 110–126) as a result of the shallower thermocline in the Costa Rica Dome region (Figs 2, S3).

Most of our data were obtained within low latitude regions (0°–40°), which Cornec et al. (2021), based on Argo float profiles, divided into two subzones, the subtropical gyres (20°–40°), with DCM mainly due to photoacclimation, and the subequatorial region (0°–10°), with DCM profiles contributed at least in part by deep biomass maxima. HPLC analyses of Chl *a* performed with samples from the same sampling depths as those used in this study (Latasa et al. 2023) showed that haptophytes and *Prochlorococcus* were the dominant contributors to total Chl *a* (36% and 35%, respectively), followed by green algae (11%), *Synechococcus* (6.5%), pelagophytes (6.7%), dinoflagellates (3.2%) and diatoms (1.6%). With the exception of diatoms and *Synechococcus*, which showed a fairly homogeneous vertical distribution in the water column, most of these groups increased their pigment contribution at or near the DCM. Enumerations of nano- and microphytoplankton by optical microscopy (Estrada et al. 2016) suggested that, globally, there were no significant differences between the mean abundances of diatoms, dinoflagellates, coccolithophores and nanoflagellates among the three light levels sampled (surface, 20% PAR and DCM). A rough estimate of the average (±SD) Chl

a content per cell (obtained by dividing the sum of Chl *a* concentrations of the micro- and nanophytoplankton fractions by the corresponding abundance of nano- and microphytoplankton cells) gave, respectively, 2.6±1.6, 3.0±2.0 and 9.1±16.8 pg cell^{-1} for the surface, 20% surface PAR and DCM samples. Regarding picophytoplankton, the proportion of <2 μm Chl *a* (Table 2) assessed by filtration was similar (or only slightly higher at the DCM) for all light levels (see below), but picophytoplankton cell counts by flow cytometry (Agustí et al. 2019), including *Prochlorococcus*, *Synechococcus* and picoeukaryotes, revealed that, in general, *Prochlorococcus* showed cell concentration maxima some tens of metres above the DCM, while *Synechococcus* were more abundant at shallower levels, and picoeukaryotes peaked at the DCM depth. A rough estimation of picoplankton carbon biomass obtained by using the conversion factors of Zamanillo et al. (2019) (51 fg C cell^{-1} for *Prochlorococcus*, 175 fg C cell^{-1} for *Synechococcus* and 1319 fg C cell^{-1} for picoeukaryotes) showed that the picophytoplankton carbon biomass maximum occurred well above the DCM at most stations (data not shown). These observations suggest that the increased Chl *a* concentration at the DCM was due to photoacclimation of the phytoplankton cells (see also Latasa et al. 2023) rather than to increases in cell biomass. Another rough indication was obtained from the relationships between particulate organic carbon (POC) concentrations (Pérez et al. 2006) and Chl *a*. The problem with this approach is that POC includes an important and variable contribution of detritus and, while some studies have found that these represent a relatively stable fraction (21%–43% for 0–200 m integrated samples for the Sargasso Sea, DuRand et al. 2001), others have reported much wider ranges (12%–97% for surface samples of diverse marine ecosystems, Graff et al. 2015). In our study, POC/Chl *a*_tot ratios for the stations with DCM that had POC data for both surface and DCM (Table S6) averaged 270.1±184.9 (SD) w/w for surface waters and 48.8±24.1 w/w for the DCM. Assuming a similar contribution of phytoplankton carbon to total POC for the surface and DCM, this would represent a mean Chl *a* content per unit cell carbon 5.5 times higher at the DCM than at the surface. This difference would be sufficient to account for the average value (5) of the ratio between Chl *a* at the DCM and Chl *a* at the surface (Table S6). These estimations further support the conclusion that the Chl *a* increase at the DCM was mostly due to photoacclimation.

The DCM depth was located below the mixed layer and was associated with the irradiance level (as seen by the relationship with the depth of 1% surface PAR, Fig. 3A), and the nutricline, represented in our study by the nitracline (Fig. 4A). This finding agrees with previous studies (Agustí and Duarte 1998, Estrada et al. 1993, Cullen 1982, Mignot et al. 2014) and with the view that the DCM, including both enhanced biomass and photoacclimation components, is generated by the interaction between vertically opposite gradients of light and nutrients (Margalef 1978), with reduced vertical mixing below the MLD allowing for vertical heterogeneity. It can be noted that, as remarked by Cullen (2015), the relevant light parameter should be related to appropriately averaged absolute irradiance values rather than to relative light levels. In our case, when we considered samples taken between 9:00 and 15:00 solar time, the instantaneous irradiance range at the DCM depth was relatively narrow, with a mean (± standard deviation) of 11.4±11.4 µmol photons m^{-2} s^{-1} (median=8.8 µmol photons m^{-2} s^{-1}).

The pattern shown in Figure 4A, where the DCM is deeper or shallower than the nitracline when it is, respectively, above or below 100 m depth, agrees with the findings of Cornec et al. (2021) and Richardson

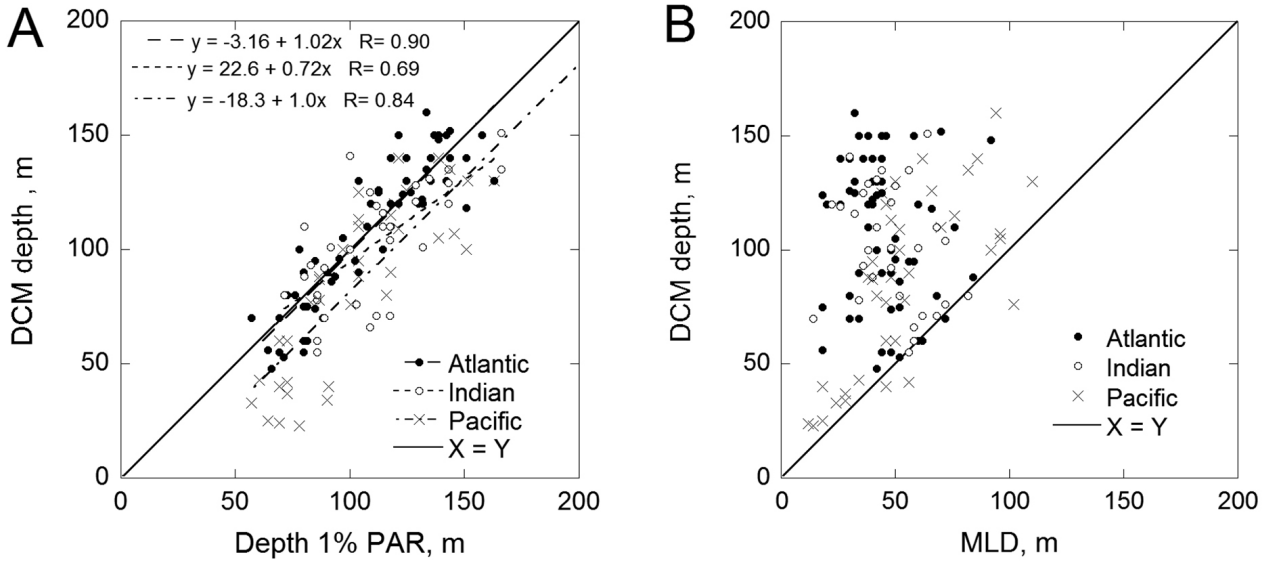

Fig. 3. – Relationship of the DCM depth with the 1% surface light level (A) and with the MLD (B). The solid line shows the 1:1 relationship. Significant regression lines (dashed) and equations are indicated.

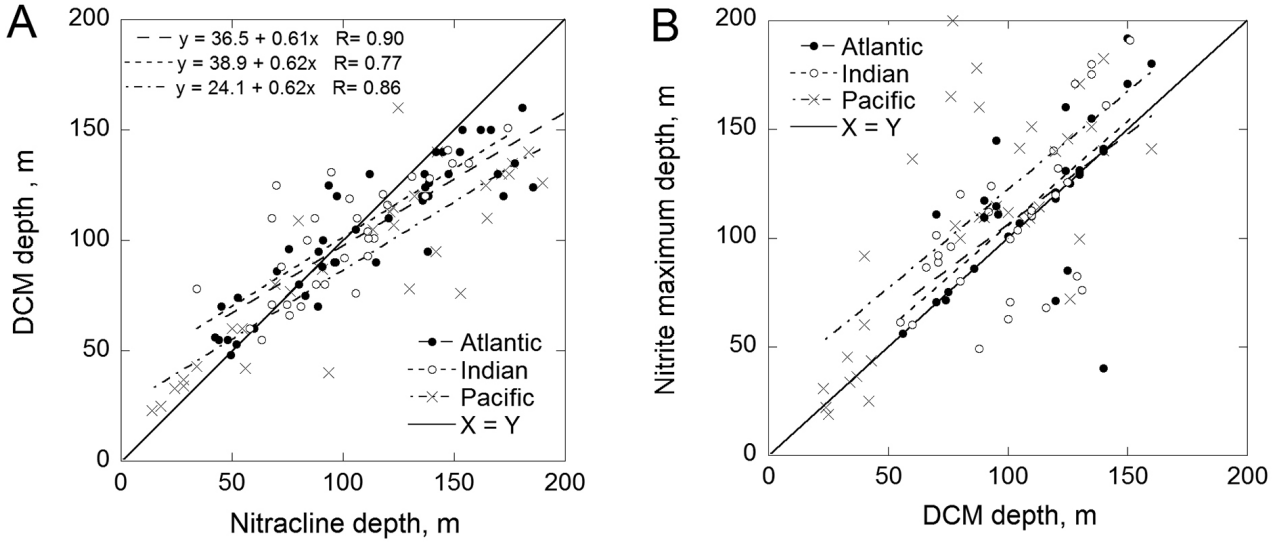

Fig. 4. – Relationship between DCM depth and nitracline depth (A) and between nitrite maximum depth and DCM depth (B). The solid line shows the 1:1 relationship. Significant regression lines (dashed) and equations (in A) are indicated. The equations in (B) are y=23.6+0.83x (correlation, R=0.64) for the Atlantic Ocean; y=10.1+0.96x (R=0.66) for the Indian Ocean and y=31.5+0.90x (R=0.69) for the Pacific Ocean.

and Bengtsen (2019). According to the latter authors, a shallower DCM than nitracline at depths below 100 m results from the interaction between light availability and the likelihood of intermittent nutrient supply from a deeper nitracline. On the other hand, a DCM deeper than the nitracline, which occured at some stations, could be explained by limitation of another nutrient, such as phosphorus, below the nitracline depth. We explored the phosphate concentration profiles to test this possibility, but the conclusions were not straightforward because phosphate gradients were less marked than those of nitrate, probably due in part to more rapid remineralization of phosphorus relative to nitrogen (Monteiro and Follows 2012). We tried two definitions of the phosphocline: A) the shallowest depth where phosphate concentrations equalled or exceeded (without interpolation) 0.35 µM (this was based on a compilation of NW Mediterranean profiles by Segura-Noguera et al. 2016); and B), the shallowest depth where phosphate concentrations equalled or exceeded 0.10 µM. As can be seen in Figure S5A and B, the phosphate concentrations ≥0.35 µM were practically always much deeper than the nitracline (original data can be consulted at https://doi.org/10.20350/digitalCSIC/16127). On the other hand, apart from several stations that had phosphate concentrations ≥0.10 µM at the surface (Fig. S5C and D), the phosphate concentrations ≥0.10 µM tended to be deeper or shallower than the nitracline (we adopted an absolute minimum difference of 10 m to define these two situations) when the DCM was respectively 10 m deeper or shallower than the nitracline. This finding supports the idea that, in certain situations, phosphorus limitation below the nitracline may lower the depth of the DCM; it also indicates that comparing the depths of the DCM and the nitracline, along with those of the clines of other nutrients, could help identify the limiting element.

The occurrence of a primary nitrite maximum at subsurface levels (Fig. 4B) has been repeatedly documented (Kiefer et al. 1976, Estrada et al. 1993, Collos 1998). The maintenance of this nitrite maximum has been attributed to both microbial nitrification and nitrite release by phytoplankton, and the relative importance of both mechanisms is still discussed, with some authors favouring the preponderance of phytoplankton excretion (Blasco 1971, Lomas and Lipschultz 2006) and others favouring nitrification by chemoautotrophs (Meeder et al. 2012, Zakem et al. 2018). Our data showed in general a nitrite maximum either deeper or coincident with the DCM, but there were some exceptions. In principle, a nitrite maximum depth coinciding with that of the DCM would suggest phytoplankton excretion, while nitrification would result in a nitrite maximum deeper than the DCM, although both mechanisms might be operative at the same time. However, as described by Lomas and Lipschultz (2006), there are a number of physical disturbance and physiological scenarios that could decouple the depths of the nitrite maximum from those of the DCM and associated variables; for example, according to these authors, a shallower nitrite maximum than the DCM could arise from transient, light-induced uncoupling of nitrate and nitrite reduction by DCM phytoplankton exposed to periodic low-level nitrate inputs or short-lived light changes at sunrise or sunset.

Non-significant (Cox et al. 1982, Estrada et al. 1993) and negative (Herbland and Voituriez 1979, Cornec et al. 2021) relationships between Chl *a*_DCM and DCM depth (Fig. 5B) have been previously documented; the latter situation may be related to increasing light limitation with depth.

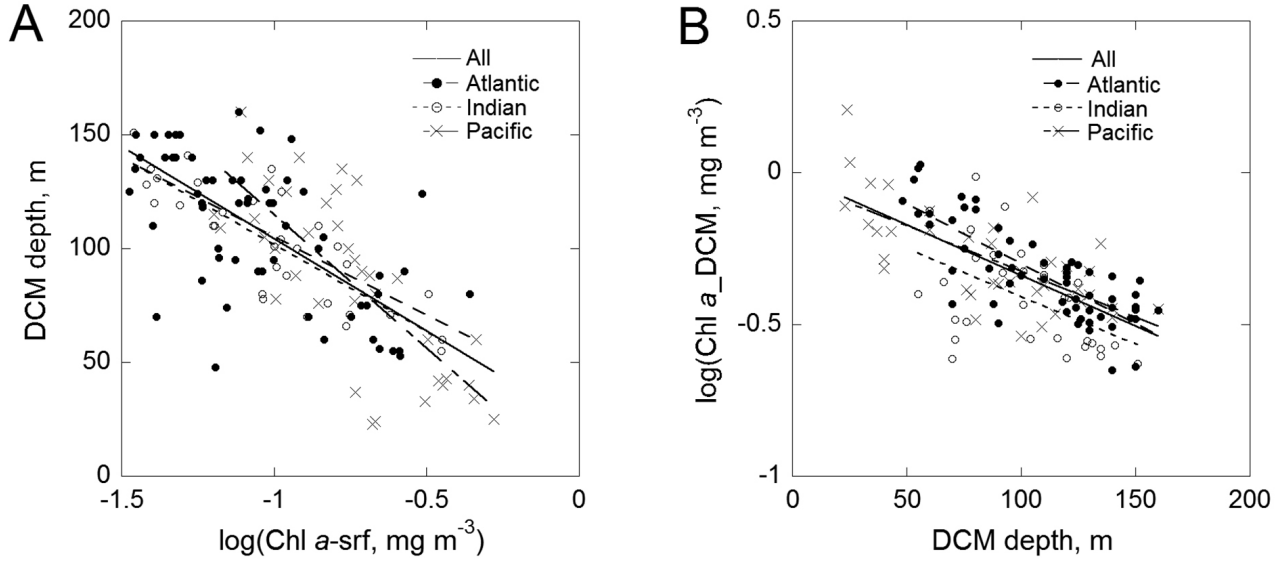

Fig. 5. – Relationship between (A) DCM depth and Chl *a* concentration at the surface [log(Chl *a*_srf)] and (B) Chl *a* concentration at the DCM [log(Chl a_DCM)] and DCM depth. The equations of the regression lines in (A) are y=36.7–68.8x (correlation, R=0.62) for the Atlantic, y=25.6–76.3x (R=0.83) for the Indian, y =-2.28–117.1x (R=0.76) for the Pacific and y=23.4–81.1x (R=0.72) for all oceans. The equations in (B) are y=0.094-0.0039x (R=0.80) for the Atlantic, y=-0.092-0.0031x (R=0.50) for the Indian, y=-0.027-0.0030x (R=0.70) for the Pacific and y=-0.0037-0.0033x (R=0.68) for all oceans.

Relationships between total and size-fractionated chlorophyll *a*

On average, picophytoplankton was the dominant contributor at all light levels, oceans and zones (Table 2); only at a few U-D locations, such as stations 90–94 (data not shown), was the picophytoplankton proportion lower than 50%. This is an expected result, given the general oligotrophic character of the sampled locations (Marañón 2009, IOCCG 2014). Picophytoplankton contribution increased with Chl *a*_pol without approaching an asymptotic value (Fig. 6A-D), as found by Agustí et al. (2019) for flow cytometry counts of *Synechococcus*, *Prochlorococcus* and picoeukaryotes. This result may be explained, at least in part, by the low values of the Chl *a* concentrations measured in the Malaspina expedition, which (except for station 45) did not reach the concentration of the inflexion point reported by other authors around 1 mg m^{-3} of total Chl *a* (Marañón et al. 2009, Brewin et al. 2019). Regarding this particular value, it should be noted tha3t many field Chl *a* data sets, including our own, are derived from fluorometric measurements, which tend to overestimate the concentration of Chl *a* as determined from HPLC, considered the technique of choice for pigment determination (Garrido and Roy 2015); for Malaspina, the relationship was Chl *a*_tot=Chl *a*_HPLC*1.34+25, r^2=0.77, where Chl *a*_HPLC is the total Chl *a* as determined by HPLC (Latasa et al. 2023). The linear correlation between our determinations of f_pico and f_micro and those derived from the Hirata equations (Fig. S3) was significant but explained only 3% of the variance for microphytoplankton and 22% for picophytoplankton, thus limiting the usefulness of this approximation, at least in data sets with relatively narrow variability.

For all light levels, the slope of f_pico with respect to log(Chl *a*_pol) was positive, while the relationships of f_nano and f_micro with log(Chl *a*_pol) were negative or non-significant (Table S5B), so f_pico increased (and f_nano and f_micro decreased or did not change significantly) with total Chl *a* (Fig. S1), in contrast with the findings of Brewin et al. (2019) when similar Chl *a* concentration ranges were considered. However, our findings must be interpreted with caution, given the strong dispersion of the regression lines related to micro- and nanophytoplankton data. Another caveat are the potential artefacts introduced by filtration, such as the effect of biomass accumulation on particle retention (Brewin et al. 2014); however, our sequential filtration methodology was similar to that employed by Brewin et al. (2019) and it is difficult to envision why higher biomass should favour pico- but not nanophytoplankton retention.

Picoplankton contribution (in particular that of cyanobacteria) has been often reported to increase with temperature (Flombaum et al. 2013). However, it must be noted that statistical relationships with temperature often result from its covariation with other variables, such as nutrient concentration (Otero-Ferrer et al. 2018, Agustí et al. 2019), rather than from any direct effects (see next section). Within the temperature range of our data set, the lack of correlation of f_pico and f_nano with temperature (data not shown) suggests that the relative contribution of these size classes was driven by factors such as resource availability, as found by Marañón (2015).

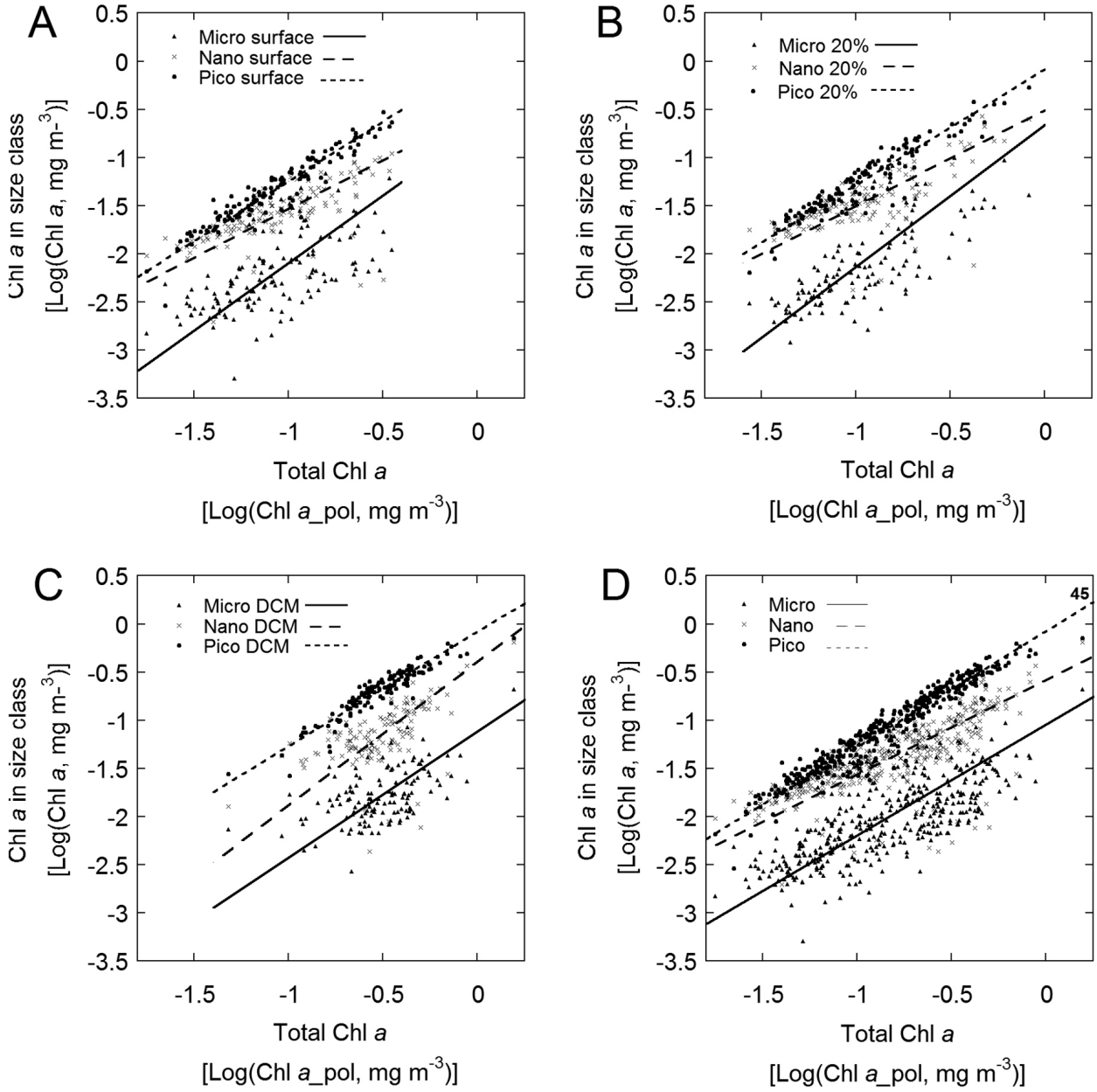

Fig. 6. – Relationships of micro-, nano- and picophytoplankton Chl *a* with the sum of Chl *a* in all three size fractions (Chl *a*_pol) for surface (A), the 20% surface PAR (B), the DCM (C) and all light levels pooled (D). The number "45" in the upper right side of Fig. 6D indicates the x position of the Chl *a* values corresponding to this station. The equations of the regression lines can be found in Table S5.

Relationships of integrated chlorophyll *a* (Chl *a*_int) with surface chlorophyll *a* (Chl *a*_srf), surface temperature and stratification

In temperate regions, high temperatures often cause increased stratification, diminishing nutrient availability in surface waters. This leads to negative correlations between both surface temperature and stratification indices, and Chl *a*_srf and integrated phytoplankton biomass estimates, which include integrated Chl *a* (Doney 2006, Behrenfeld et al. 2006, van de Poll et al. 2013). In our latitudinally-restricted data set, the best predictor of Chl *a*_int for the global data set and for the various oceans and regions was Chl *a*_srf (Table S4). Correlation coefficients of SST and σ200-σ6 with Chl *a*_srf or Chl *a*_int were mostly non-significant. Negative correlations were found only between SST and Chl *a*_srf for the Indian Ocean and between SST and Chl *a*_int for the tropical region (Table 3). These findings agree with those of Dave and Lozier (2013), who compared estimates of stratification (from hydrographic profiles) and Chl *a* (from satellite) for the global tropical and

subtropical oceans. They found that a negative relationship was valid for globally averaged data at interannual time scales but broke down at the basin scale. As potential explanations for these results, they pointed out that stratification by itself does not predetermine the strength of vertical mixing and that lateral inputs of nutrients from other locations could also be important. Another example of different patterns depending on the scale of observation is reported by Barton et al. (2014), based on the Continuous Plankton Recorder and accompanying observations. They concluded that physical mechanisms, such as turbulent mixing, differentiated the fates of diatoms and dinoflagellates on seasonal timescales, but did not appear to drive their longer-term variability. In our analysis, we could add the relatively small range of temperatures in the visited regions and the confounding effect of pooling together data from various water masses with different SST, stratification and phytoplankton productivity backgrounds and temporal histories. In fact, for each of the three light levels, temperature (Table S7) was significantly lower in the Indian Ocean than in the Atlantic or the Pacific (ANOVA, $p<0.0001$, and Tuckey test, n=32-60), while σ200-σ6, Chl *a*_DCM and Chl *a*_int (Table 1) were higher for the Pacific than for the other oceans (ANOVA, $p<0.0001$, and Tuckey tests, n=32-61). The implication is that global relationships of phytoplankton variables with temperature or local stratification indices as indicators of nutrient fluxes and phytoplankton growth in the surface layer must be critically assessed taking into account the structure of each data set.

CONCLUSIONS

The Malaspina-2010 circumnavigation expedition surveyed tropical and subtropical regions of the Atlantic, Indian and Pacific oceans mostly during the spring-summer months of the visited areas. In general, there was a marked temperature stratification, a DCM was found at most stations between 60 and 150 m depth, and a nitrite maximum occurred at depths similar to or deeper than the DCM; the exceptions were several areas affected by upwelling or divergences: the Atlantic and Pacific equatorial upwellings, the Costa Rica Dome and the Eastern Great Australian Bight. Typically, the DCM was located close to the level of 1% PAR, was deeper than the MLD and occurred either at the same depth as or a few metres above the nitracline. The linear regression equations of DCM depth on nitracline depth were positive and significant and had similar slopes for all three oceans. These findings agree with the description of the "typical tropical structure" (Herbland and Voituriez 1979) or the "typical stable water structure" (Cullen 2015) and support the idea that, at least across tropics and subtropics, the DCM occurrence is shaped by a similar interplay of light and nutrient gradients.

In contrast with results reported in other studies, the proportion of picophytoplankton Chl *a* (f_pico) was significantly higher at the DCM and increased with total Chl *a* (Chl *a*_pol) while f_nano and f_micro decreased. Higher cell pigment content due to photoacclimation appeared to be the most important contributor to the DCM.

The significant correlation of Chl *a*_int with Chl *a*_srf, with linear regression slopes that were not significantly different among the studied oceans or geographical zones, supports the feasibility of using remote sensing of surface Chl *a* to derive information on integrated Chl *a* concentration in the water column of these regions. In contrast, Chl *a*_srf was negatively correlated with SST and the σ200-σ6 stratification in-

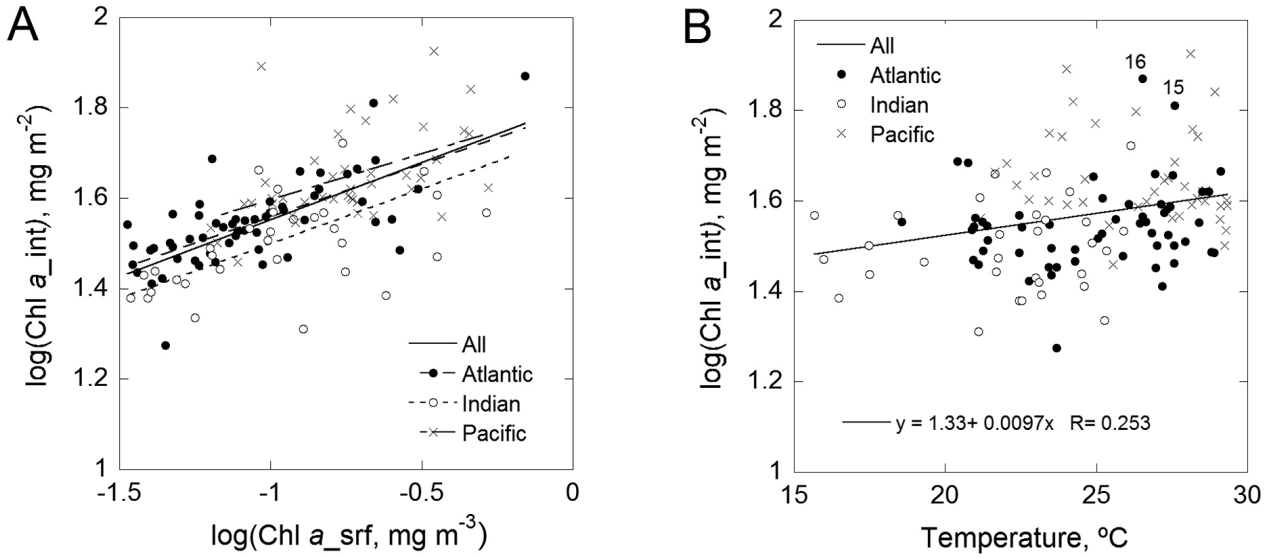

Fig. 7. – Relationship of integrated Chl *a* (Chl *a*_int) with Chl *a* at the surface (Chl *a*_srf), (A) and with sea surface temperature (B). Significant regression lines are shown. The equations in (A) are y=1.79+0.23x (correlation, R=0.69) for the Atlantic, y=1.74+0.24x (R= 0.62) for the Indian, y=1.80+0.20x (R=0.48) for the Pacific and y=1.81+0.25x (R=0.66) for all oceans.

dex only for the Indian Ocean, highlighting the need for caution in relating increased temperature or stratification to decreased pigment concentration.

SUPPLEMENTARY MATERIAL

The following supplementary material is available through the online version of this article:

Fig. S1. Relationship between the logarithm of the sum of Chl *a* for all size fractions [log(Chl *a*_pol)] and the proportion of Chl *a* in the microphytoplankton (f_micro), nanophytoplankton (f_nano) and picophytoplankton (f_pico) at surface (A), the 20% light level (B), the DCM level (C) and all light levels pooled (D). The equations of the RMA regression lines (only the significant ones are shown) can be found in Table S5.

Fig. S2. Relationship between the measured proportions of Chl *a* in the micro- and picophytoplankton size fractions and calculated according to the Hirata algorithm (Hirata f_micro and Hirata f_pico, respectively). The equations are y=0.10-0.17x (correlation, R=0.19) for Hirata f_micro and y=0.68-0.39x (R=0.48) for Hirata f_pico.

Fig. S3. Spatial variability of surface Chl *a* (Chl *a*_srf) and integrated Chl *a* (Chl *a*_int) along the Malaspina-2010 cruise track.

Fig. S4. Salinity (A) and potential density anomaly (σ0, kg m^{-3}, panel B) distributions during the Malaspina-2010 expedition. The white lines indicate the mixed layer depth. The initial and final stations of each leg and the different regions indicated in Fig. 1, are shown on top of the (A) panel.

Fig. S5. Relationships between the nitracline depth and the shallower depth with phosphate concentrations equal or exceeding 0.35 mmol m^{-3} (A, B) or 0.10 mmol m^{-3} (C, D). Stations with DCM more than 10 m deeper than the nitracline are marked with "1" and those with DCM more than 10 m shallower than the nitracline are marked with "2" (the 10 m absolute difference between DCM and nitracline was adopted to account for uncertainties in the sampling depths).

Table S1. Oceans and zones visited during the seven legs of the Malaspina-2010 expedition.

Table S2. Cruise schedule of Malaspina 2010.

Table S3. Parameters of the linear regression equations of the DCM depth on the nitracline depth (m) for the different oceans and zones and for the whole data set ("All").

Table S4. Parameters of significant linear regression equations between different dependent and independent variables for the different oceans and zones, and for the whole data set. (A) Regression of the logarithms of integrated Chl *a* concentration [log(Chl *a*_int)] on the Chl *a* concentration at surface [log(Chl *a*_srf)]. (B) Regressions of log(Chl *a*_srf) and log(Chl *a*_int) on sea surface temperature (SST) and the σ200-σ6 stratification index. (C) Regression of the logarithm of Chl *a* concentration at the DCM [log(Chl *a*_DCM)] on the DCM depth for the depth intervals 0 -200 m, 0-100 m and 100-200 m.

Table S5. (A) Parameters of the RMA regression equations of the logarithm of the Chl *a* concentration in the micro- [log(Chl *a*_micro)], nano- [log(Chl a_nano)] and picophytoplankton [log(Chl *a*_pico)] size fractions on the logarithm of the total Chl *a* concentration, calculated as the sum of all the fractions [log(Chl *a*_pol)], for the different light levels. (B) Parameters of the RMA regression equations of the fractional (per unit) contribution of micro- (f_micro), nano- (f_nano) and picophytoplankton (f_pico) on Chl *a*_pol, for the different light levels.

Table S6. Particulate organic carbon (POC, μM), Chl *a*_tot concentrations, POC/Chl *a*_tot ratios for surface and DCM, and ratio between Chl *a*_tot at DCM (Chl *a*_DCM) and Chl *a*_tot at surface (Chl *a*_srf). surface. Only stations with DCM and for which both POC and Chl *a*_tot data from surface and DCM were available have been used.

Table S7. Statistical parameters of the temperature for the three light levels in the Atlantic, Indian and Pacific oceans.

ACKNOWLEDGEMENTS

This work was supported by Consolider- Ingenio 2010, CSD2008-00077 of the former Spanish Ministerio de Ciencia e Innovación and the Consejo Superior de Investigaciones Científicas (CSIC) of Spain. We are grateful to C.M. Duarte for the coordination of the project and to S. Agustí for leading the phytoplankton research block. Dr. Irene Teixidor-Toneu (Institut Méditerranéen de Biodiversité et d'Écologie Marine et Continentale, Marseille, France) contributed to nutrient sampling and analysis during the cruise.

FUNDING SOURCES

Project Consolider- Ingenio 2010, CSD2008-00077 of the former Ministerio de Ciencia e Innovación, Spain. Consejo Superior de Investigaciones Científicas (CSIC), Spain.

AUTORSHIP CONTRIBUTION

Marta Estrada: Conceptualization, Data curation, Formal analysis, Investigation, Methodology, Supervision, Writing—original draft, Writing—review and editing.

Mikel Latasa: Conceptualization, Data curation, Investigation, Methodology, Supervision, Writing—review and editing

Ana María Cabello: Data curation, Investigation, Writing—review and editing

Patricia de la Fuente: Data curation, Investigation, Writing—review and editing

Carles Guallar: Data curation, Investigation, Writing—review and editing

Patricija Mozetič: Data curation, Investigation, Writing—review and editing

Max Riera-Lorente: Data curation, Investigation, Writing—review and editing

Montserrat Vidal: Conceptualization, Data curation, Funding acquisition, Investigation, Methodology, Supervision, Writing—review and editing

Dolors Blasco: Conceptualization, Data curation, Formal analysis, Funding acquisition, Investigation, Methodology, Supervision, Writing—review and editing

REFERENCES

Agustí S., Duarte C.M. 1998. Phytoplankton chlorophyll a distribution and water column stabillity in the central Atlantic Ocean. Oceanol. Acta, 22(2): 193-203. https://doi.org/10.1016/S0399-1784(99)80045-0

Agustí S., Lubián L.M., Moreno-Ostos E., Estrada M., Duarte C.M. 2019. Projected changes in photosynthetic picoplankton in a warmer subtropical ocean. Front. Mar. Sci. 5: 506. https://doi.org/10.3389/fmars.2018.00506

Antoine D., André J-M., Morel A. 1996. Oceanic primary production 2. Estimation at global scale from satellite (coastal zone color scanner) chlorophyll. Global Biogeochem. Cy. 10: 57-69. https://doi.org/10.1029/95GB02832

Barton A.D., Lozier M.S., Williams R.G. 2014. Physical controls of variability in North Atlantic phytoplankton communities. Limnol. Oceanogr. 60: 181-197. https://doi.org/10.1002/lno.10011

Barton A.D., Pershing A.J., Litchman E., Record N.R., Edwards K.F., Finkel Z.V., Kiørboe T., Ward B.A. 2013. Ecology Letters, 16: 522-534 https://doi.org/10.1111/ele.12063

Behrenfeld M.J., Boss E.M., Siegel D.A., Shea D.M. 2006. Carbon-based ocean productivity and phytoplankton physiology from space. Global Biogeochem. Cycles, 19: GB1006. https://doi.org/10.1029/2004GB002299

Behrenfeld M.J., O'Malley R.T., Siegel D.A., McClain C.R., Sarmiento, J.L. Feldman G.C., Milligan A.J., Falkowski P.G., Letelier R.M., Boss E.S. 2006. Climate-driven trends in contemporary ocean productivity Nature, 444(7120): 752-755. https://doi.org/10.1038/nature05317

Blasco D. 1971. Acumulación de nitritos en determinados niveles marinos por acción del fitoplancton. PhD. Thesis, Universitat de Barcelona, 223 pp.

Blasco D., De La Fuente Gamero P., Galindo M. 2012. Muestreo y análisis de nutrientes inorgánicos disueltos en agua de mar. In: Moreno-Ostos E. (ed), Expedición de circunnavegación Malaspina 2010: cambio global y exploración de la biodiversidad del océano. Libro blanco de métodos y técnicas de trabajo oceanográfico. CSIC, Madrid, pp. 107-121. http://hdl.handle.net/10261/316257

Brewin R.J.W., Morán X.A.G., Raitsos D.E., Gittings J.A., Calleja M.L.l., Viegas M., Ansari M.I., Al-Otaibi N., Huete-Stauffer T.M., Hoteit I. 2019. Factors Regulating the Relationship Between Total and Size-Fractionated Chlorophyll-a in Coastal Waters of the Red Sea. Front. Microbiol. 10: 1964. https://doi.org/10.3389/fmicb.2019.01964

Brewin R.J.W., Sathyendranath S., Hirata T., Lavender S.J., Barciela R., Hardman- Mountford, N.J. 2010. A three-component model of phytoplankton size class for the Atlantic Ocean. Ecol. Model. 221: 1472-1483. https://doi.org/10.1016/j.ecolmodel.2010.02.014

Brewin R.J.W., Sathyendranath S., Lange P.K., Tilstone G. 2014. Comparison of two methods to derive the size-structure of natural populations of phytoplankton. Deep Sea Res. I, 85: 72-79. https://doi.org/10.1016/j.dsr.2013.11.007

Browning T.J., Moore M.C. 2023. Global analysis of ocean phytoplankton nutrient limitation reveals high prevalence of co-limitation. Nat. Comm. 14: 5014. https://doi.org/10.1038/s41467-023-40774-0

Collos Y. 1998. Nitrate uptake, nitrite release and uptake, and new production estimates. Mar. Ecol. Prog. Ser. 171: 293-301. https://doi.org/10.3354/meps171293

Cornec M., Claustre H., Mignot A., Guidi L., Lacour L., Poteau A., D'Ortenzio F., Gentili B., Schmechtig C. 2021. Deep chlorophyll maxima in the global ocean: Occurrences, drivers and characteristics. Global Biogeochem. Cy. 35: e2020GB006759. https://doi.org/10.1029/2020GB006759

Cox J.L., Wiebe P.H., Ortner P, Boyd S. 1982. Seasonal development of subsurface chlorophyll maxima in Slope Water and Northern Sargasso Sea of the Northwestern Atlantic Ocean. Biol. Oceanogr. 1: 271-285.

Cullen J.J. 2015. Subsurface Chlorophyll Maximum Layers: Enduring Enigma or Mystery Solved? Annu. Rev. Mar. Sci. 7: 207-239. https://doi.org/10.1146/annurev-marine-010213-135111.

Cullen J.J. 1982. The deep chlorophyll maximum: Comparing vertical profiles of Chlorophyll a. Can. J. Fish. Aquat. Sci. 39:791-803. https://doi.org/10.1139/f82-108.

Dave A.C, Lozier M.S. 2013. Examining the global record of interannual variability in stratification and marine productivity in the low-latitude and mid-latitude ocean. J. Geophys. Res. Oceans 118: 3114-3127. https://doi.org/10.1002/jgrc.20224

Doney S.C. 2006. Plankton in a warmer world. Nature 444: 595-596. https://doi.org/10.1038/444695a

DuRand M.D., Olson R.J., Chisholm S.W. 2001, Phytoplankton population dynamics at the Bermuda Atlantic Time-series station in the Sargasso Sea, Deep-Sea Res. Part II 48: 1983- 2003. https://doi.org/10.1016/S0967-0645(00)00166-1

Estrada M. 2012. Determinación fluorimétrica de la concentración de clorofila a. In: Moreno-Ostos E. (ed), Expedición de circunnavegación Malaspina 2010: cambio global y exploración de la biodiversidad del océano. Libro blanco de métodos y técnicas de trabajo oceanográfico. CSIC, Madrid, pp. 399-405. http://hdl.handle.net/10261/316257

Estrada M., Delgado M., Blasco D., Latasa M., Cabello A.M., Benítez-Barrios V., Fraile-Nuez E., Mozetič P., Vidal M. 2016. Phytoplankton across Tropical and Subtropical Regions of the Atlantic, Indian and Pacific Oceans. PLoS ONE 11(3): e0151699. https://doi.org/10.1371/journal.pone.0151699

Estrada M., Marrasé C., Latasa M., Berdalet E., Delgado M., Riera T. 1993. Variability of deep chlorophyll maximum characteristics in the Northwestern Mediterranean. Mar. Ecol. Prog. Ser. 92: 289-300. https://doi.org/10.3354/meps092289

Estrada M., Latasa M., Emelianov M., Gutiérrez-Rodríguez A., Fernández-Castro B., Isern-Fontanet J., Mouriño-Carballido B., Salat J., Vidal M. 2014. Seasonal and mesoscale variability of primary production in the deep winter-mixing region of the NW Mediterranean. Deep-Sea Res. Part I 94: 45-61. https://doi.org/10.1016/j.dsr.2014.08.003

Fiedler C., Talley L.D. 2006. Hydrography of the eastern tropical Pacific: a review. Prog. Oceanogr. 69: 143-180. https://doi.org/10.1016/j.pocean.2006.03.008.

Field C.B., Behrenfeld M.J., Randerson J.T., Falkowski P. 1998. Primary production of the biosphere: Integrating terrestrial and oceanic components. Science 281: 237-240. https://doi.org/10.1126/science.281.5374.237

Finkel Z.V., Beardall J., Flynn K., Quigg A., Rees T.A.V., Raven J.A. 2010. Phytoplankton in a changing world: cell size and elemental stoichiometry. J. Plank. Res. 32: 119-137. https://doi.org/10.1093/plankt/fbp098

Flombaum P., Gallegos J.L., Gordillo R.A., Rincon J., Zabala L.L., Jiao N., Karl D.M., Li W.K.W., Lomas M.W., Veneziano D. 2013. Present and future global distributions of the marine Cyanobacteria Prochlorococcus and Synechococcus. PNAS 110: 9824-9829. https://doi.org/10.1073/pnas.1307701110

Garrido, J.L., Roy S. 2015. The Use of HPLC for the Characterization of Phytoplankton Pigments. In: Dagmar B. Stengel and Solène Connan (eds), Natural Products From Marine Algae: Methods and Protocols, Methods in Molecular Biology, vol. 1308, pp. 241-251, Springer Science+Business Media New York. https://doi.org/10.1007/978-1-4939-2684-8_15.

Graff J.R., Westberry T.K., Milligan A.J., Brown M.B., Dall'Olmo G., van Dongen-Vogels V., Reifel K.M., Behrenfeld M.J. 2015. Analytical phytoplankton carbon measurements spanning diverse ecosystems. Deep-Sea Res. Part I, 102: 16-25. https://doi.org/10.1016/j.dsr.2015.04.006

Grasshoff K., Kremling K., Erhardt M. (eds) 1999. Methods of Seawater Analysis. Wiley-VCH, Weinheim, 632 pp.Guidi L., Chaffron. S., Bittner L., Eveillard. D., Larhlimi. A., Roux S., Gorsky G. 2016. Plankton networks driving carbon export in the oligotrophic ocean, Nature 532(7600): 465-470. https://doi.org/10.1038/nature16942

Herbland A., Voituriez B. 1979. Hydrological structure analysis for estimating the primary production in the tropical Atlantic Ocean. J. Mar. Res. 37: 87-101.

Hirata T., Aiken J., Hardman-Mountford N., et al. 2008. An absorption model to determine phytoplankton size classes from satellite ocean colour. Remote Sens. Environ. 112: 3153-3159. https://doi.org/10.1016/j.rse.2008.03.011
Hirata T., Hardman-Mountford N.J., Brewin R.J.W., et al. 2011. Synoptic relationships between surface chlorophyll a and diagnostic pigments specific to phytoplankton functional types. Biogeosciences 8: 311-327. https://doi.org/10.5194/bg-8-311-2011
IOCCG (2014). Phytoplankton Functional Types from Space. Technical report. Sathyendranath S. (ed), Reports of the International Ocean-Colour Coordinating Group, No. 15, IOCCG, Dartmouth, NS.
Kiefer D.A., Olson R.J., Holm-Hansen O. 1976. Another look at the nitrite and chlorophyll maxima in the central North Pacific. Deep-Sea Res. 23: 1199-1208. https://doi.org/10.1016/0011-7471(76)90895-0
Latasa M., Rodríguez F., Agustí S., Estrada M. 2023. Distribution patterns of phytoplankton groups along isoirradiance layers in oligotrophic tropical and subtropical oceans. Prog. Oceanogr. 217: 103098. https://doi.org/10.1016/j.pocean.2023.103098
Latasa M., Morán X.A.G., Scharek R., Estrada M. 2005. Estimating the carbon flux through main phytoplankton groups in the northwestern Mediterranean. Limnol. Oceanogr. 50: 1447-1458. https://doi.org/10.4319/lo.2005.50.5.1447
Levitus S. 1982. Climatological Atlas of the World Ocean. NOAA Professional Paper 13. Rockville, Md, USA: U.S. Department of Commerce, National Oceanic and Atmospheric Administration. 173 pp.
Lomas M.V., Lipschultz F. 2006. Forming the primary nitrite maximum: Nitrifiers or phytoplankton? Limnol. Oceanogr. 51: 2453-2467. https://doi.org/10.4319/lo.2006.51.5.2453
Marañón E. 2009. Phytoplankton size structure. Encyclopedia of Ocean Sciences (Second Edition). Academic Press, pp. 445-452. https://doi.org/10.1016/B978-012374473-9.00661-5
Marañón, E. 2015. Cell Size as a key determinant of phytoplankton metabolism and community structure. Annu. Rev. Mar. Sci. 7: 241-264. https://doi.org/10.1146/annurev-marine-010814-015955
Meeder E., MacKey K. R. M., Paytan A., Shaked Y., Iluz D., Stambler N., Rivlin T., Post A.F., Lazar, B. 2012. Nitrite dynamics in the open ocean-clues from seasonal and diurnal variations. Mar. Ecol. Prog. Ser. 453: 11-26. https://doi.org/10.3354/meps09525
Mignot A., Claustre H., Uitz J., Poteau A., D'Ortenzio F., Xing X. 2014. Understanding the seasonal dynamics of phytoplankton biomass and the deep chlorophyll maximum in oligotrophic environments: A Bio-Argo float investigation. Global Biogeochem. Cy. 28: 856-876. https://doi.org/10.1002/2013GB004781
Monteiro F.M, Follows M.J. 2012, On nitrogen fixation and preferential remineralization of phosphorus. Geophys. Res. Lett., 39: L06607. https://doi.org/10.1029/2012GL050897
Moreno-Ostos E. (ed) 2012. Expedición de circunnavegación Malaspina 2010: cambio global y exploración de la biodiversidad del océano. Libro blanco de métodos y técnicas de trabajo oceanográfico. CSIC, Madrid, Spain, 698 pp. http://hdl.handle.net/10261/316257
Otero-Ferrer J.L., Cermeño P., Bode A., Fernández-Castro B., Gasol J.M., Morán X.A.G., Marañon E., Moreira-Coello V., Varela M.M., Villamaña M., Mouriño-Carballido B. 2018. Factors controlling the community structure of picoplankton in contrasting marine environments, Biogeosciences 15: 6199-6220, https://doi.org/10.5194/bg-15-6199-2018
Paternoster R., Brame R., Mazerolle P., Piquero A. 1998. Using the correct statistical test for the equality of regression coefficients. Criminology 36: 859-866. https://doi.org/10.1111/j.1745-9125.1998.tb01268.x.
Pérez V., Fernández E., Marañ'n E., Morán X.A.G., Zubkov, M.V. 2006. Vertical distribution of phytoplankton biomass, production and growth in the Atlantic subtropical gyres. Deep-Sea Res. Part I 53: 1616-1634 https://doi.org/10.1016/j.dsr.2006.07.008
Platt T., Denman K.L. 1978. The structure of pelagic marine ecosystems. Rapp. p.-v. réun. - Cons. int. explor. mer. 173: 60-65.
Richardson K., Bendtsen J. 2019. Vertical distribution of phytoplankton and primary production in relation to nutricline depth in the open ocean. Mar. Ecol. Prog. Ser. 620: 33-46. https://doi.org/10.3354/meps12960
Schlitzer R. 2023. Ocean Data View, odv.awi.de.
Segura-Noguera M., Cruzado A., Blasco D. 2016. The biogeochemistry of nutrients, dissolved oxygen and chlorophyll *a* in the Catalan Sea (NW Mediterranean Sea). Sci. Mar. 73: 39-56. https://doi.org/10.3989/scimar.04309.20A
Steele J.H. 1964. A study of production in the Gulf of Mexico. J. Mar. Res. 22: 211–222.
Taylor A.G., Landry M.R., Selph K.E., Wokuluk J.J. 2014. Temporal and spatial patterns of microbial community biomass and composition in the Southern California Current Ecosystem. Deep-Sea Res. II. https://doi.org/10.1016/j.dsr2.2014.02.006
van de Poll W.H., Kulk G., Timmermans K.R., Brussaard C.P.D., van der Woerd H.J., Kehoe M.J., Mojica K.D.A., Visser R.J.W., Rozema P.D., Buma A.G.J. 2013. Phytoplankton chlorophyll a biomass, composition, and productivity along a temperature and stratification gradient in the northeast Atlantic Ocean. Biogeosciences. 10: 4227-4240. https://doi.org/10.5194/bg-10-4227-2013
van Ruth P.D., Patten N.L., Doubella M.J., Piers Chapman P., Redondo Rodriguez A., Middleton J.F. 2018. Seasonal- and event-scale variations in upwelling, enrichment and primary productivity in the eastern Great Australian Bight. Deep-Sea Res. Part II 157-158: 36-45. https://doi.org/10.1016/j.dsr2.2018.09.008
Vidal M., Teixidor I., Galindo M. 2012. Muestreo de nutrientes inorgánicos disueltos (DIN), nitrógeno (TN) y fósforo (TP) totales. In: Moreno-Ostos E. (ed), Expedición de circunnavegación Malaspina 2010: cambio global y exploración de la biodiversidad del océano. Libro blanco de métodos y técnicas de trabajo oceanográfico. CSIC, Madrid, pp. 103-106. http://hdl.handle.net/10261/316257
Weingartner T.J., Weisberg R.H. 1991. On the Annual Cycle of Equatorial Upwelling in the Central Atlantic Ocean. J. Phys. Oceanogr. 21: 68-82. https://doi.org/10.1175/1520-0485(1991)021<0068:OTACOE>2.0.CO;2
Wyrtki K. 1981. An Estimate of Equatorial Upwelling in the Pacific. J. Phys. Oceanogr. 11: 1205-1214. https://doi.org/10.1175/1520-0485(1981)011<1205:AEOEUI>2.0.CO;2
Zakem E.J., Al-Haj A., Church M.J., van Dijken G.L., Dutkiewicz S., Foster S.Q., Fulweiler R.W., Mills M.M., Follows M.J. 2018. Ecological control of nitrite in the upper ocean. Nat. Commun. 9: 1206. https://doi.org/10.1038/s41467-018-03553-w
Zamanillo M., Ortega-Retuerta E., Nunes S., Rodríguez-Ros P., Dall'osto M., Estrada M., Sala M.M., Simó R. 2019. Main drivers of transparent exopolymer particle distribution across the surface Atlantic Ocean. Biogeosciences 16: 733-749. https://doi.org/10.5194/bg-16-733-2019
Zhang D., Wang C., Liu Z., Xu X., Wang X., Zhou Y. 2012. Spatial and temporal variability and size fractionation of chlorophyll a in the tropical and subtropical Pacific Ocean. Acta Oceanol. Sin. 31: 120-131. https://doi.org/10.1007/s13131-012-0212-1

GLOSSARY

B-V frequency	Brunt-Väisälä frequency
Chl *a*	Chlorophyll *a*
Chl *a*_CTD	Chlorophyll *a* concentrations calculated from CTD in situ fluorescence readings (see Material and methods)
Chl *a*_DCM	Chlorophyll *a* concentration at the deep chlorophyll maximum
Chl *a*_CTD-int	Interpolated values of Chl *a*_CTD
Chl *a*_int	Vertically integrated chlorophyll *a* concentration, between 0 and 200 m
Chl *a*_lin	Chlorophyll *a* concentration at high-resolution depth intervals, calculated by linear interpolation (see Material and methods)
Chl *a*_pol	Sum of chlorophyll *a* concentration of size categories >20 µm, >2 and <20 µm, >0.2 and <2 µm collected by sequential filtration on polycarbonate filters

Chl *a*_srf	Chlorophyll *a* at the surface (3 m depth)
Chl *a*_tot	Total chlorophyll *a* measured using GF/F filters
Chl a_tot-int	Interpolated values of Chl *a*_tot
CTD	Conductivity-temperature-depth probe
DCM	Deep chlorophyll maximum
f_micro	Fractional (per unit) contribution of microphytoplankton (>20 μm)
f_nano	Fractional (per unit) contribution of nanophytoplankton (>2 and <20 μm)
f_pico	Fractional (per unit) contribution of picophytoplankton (>0.2 and <2 μm)
MLD	Mixed layer depth
PAR	Photosynthetically active radiation
RMA	Reduced major axis linear regression
SST	Sea surface temperature
U-D regions	Upwelling-divergence regions
σ200-σ6	Difference between the potential density anomalies (with reference pressure of 0 dbar) at 200 and 6 m depth
$\sigma_\theta(z)$	Potential density anomaly at depth z (m)
Chl *a*_HPLC	Total chlorophyll *a* concentration as determined by HPLC